On the Optimal Use of Submerged Dipoles for the Generation of Unsteady Nonlinear Waves

David Le Touzé & Pierre Ferrant

Division Hydrodynamique Navale/Laboratoire de Mécanique des Fluides
École Centrale de Nantes, B.P. 92101, F-44321 Nantes Cedex 3, France
e-mail: pierre.ferrant@ec-nantes.fr *web*: http://www.ec-nantes.fr/dhn

ABSTRACT

This paper addresses the problem of unsteady wave generation and propagation in numerical wave tanks. $2D$ fully-nonlinear steep wave patterns are at interest, first in the case of regular waves, and then for obtaining prescribed focused wave packets. The wave generation process is simulated by means of an original method, involving an unsteady submerged dipole included in our recently developed pseudospectral model for fully-nonlinear free surface flows in finite water depth. Based on linear theory, an optimization of the dipole strength and orientation at a given frequency is proposed, so as to generate waves in a single direction only; unidirectional regular wave trains of different steepness are shown. Using the linear transfer function of the dipole, this optimization is then extended to the reproduction of any target wave pattern, by means of an unsteady dipole accounting for all the frequency components in the signal. The effects of nonlinearities in the fully-nonlinear temporal generation process are studied on the illustrative case of a focused wave packet.

KEY WORDS: Fully-nonlinear wave generation, Spectral method, Submerged dipoles, Focusing.

INTRODUCTION

Unlike other methods more commonly used in hydrodynamics, the pseudospectral approach is global, which means that the numerical solution is not based on a discretization of the physical domain, but expanded in terms of orthogonal functions known everywhere. Moreover the accuracy of the solution grows nearly exponentially with the number of functions kept in the expansion; this behavior is referred to as the 'spectral convergence'. Among others, examples of spectral methods applied to free surface flows include Dommermuth & Yue [1] first, and more recently Yeung & Yu [2] in an annular viscous flow domain, or Le Touzé *et al* [3] for simulations of a $3D$ numerical wave tank at second order.

The drawback of the model is to be found in its limitation to (a priori) fixed-geometry fluid domains. To overcome this limitation, a wave generation process using submerged dipoles is employed and optimized in the present paper. Verified on regular waves, it is then extended to the case of focusing wave trains, which is of particular interest for offshore design and operation. The ringing effect on structures passed a focused wave peak, especially, is a critical issue under investigation (see e.g. Grue & Huseby [4]). The coupling of the present method to a $3D$ diffraction code will lead us in the near future to a closer examination of that effect.

FORMULATION

Fully-Nonlinear Pseudospectral Modelling

A two-dimensional tank of water depth h and length L_x, partially filled with an inviscid fluid is considered. All the formulation and results presented are nondimensionalized with respect to this water depth, and to the acceleration of gravity g. Under the potential-flow theory assumption, the governing equation for the unknown velocity potential $\phi(\mathbf{M}(x,z),t)$ in the whole fluid domain D is Laplace's equation (1). The free surface is described through a classical single-valued representation at every time: $z=\eta(x,t)$. Thus, the nondimensional kinematic and dynamic conditions at the free surface FS write as (2),(3) where $\nu(x)$ is an absorption coefficient used to avoid reflections on the side walls of the tank.

$$\Delta\phi(\mathbf{M},t) = 0 \quad , \quad \mathbf{M}\in D \tag{1}$$

$$\frac{\partial\eta}{\partial t}(\mathbf{M},t) = \frac{\partial\phi}{\partial z} - \frac{\partial\phi}{\partial x}\frac{\partial\eta}{\partial x} \quad , \quad \mathbf{M}(x,\eta)\in FS \tag{2}$$

$$\frac{\partial\phi}{\partial t}(\mathbf{M},t) = -\eta - \frac{1}{2}\left(\frac{\partial\phi}{\partial x}^2 + \frac{\partial\phi}{\partial z}^2\right) - \nu(x)\frac{\partial\phi}{\partial z} \quad , \quad \mathbf{M}(x,\eta)\in FS \tag{3}$$

On the tank walls and bottom the potential ϕ has to satisfy homogeneous Neumann conditions; initially the fluid is at rest.

In order to be able to generate waves in the tank of fixed geometry, the potential ϕ is considered as the superposition of, on one hand a pseudospectral potential accounting for the tank with its free surface, and analytically-known source terms used to generate the waves on the other hand: $\phi(\mathbf{M},t)=\phi^{tank}(\mathbf{M},t)+\phi^{dipoles}(\mathbf{M},t)$ in D. The pseudospectral part is formulated as a (truncated) expansion in series of natural modes of the tank

$$\phi^{tank}(\mathbf{M},t) = \sum_{m=0}^{N_\phi} a_m(t)\cos(k_m x)\frac{\cosh(k_m(z+1))}{\cosh(k_m)} \quad , \quad \mathbf{M}\in D \tag{4}$$

with respectively $k_m = m\pi/L_x$ the wavenumber of the m^{th} mode, and $a_m(t)$ its unknown 'modal time amplitude'; N_ϕ being the order of truncation of modal series.

Wave Generation Source Terms

Monochromatic case. The source terms chosen to generate waves are submerged dipoles. This choice will allow us to generate *unidirectional* waves. To do so we study the linear solution of the wave field created by a submerged Kelvin dipole. The potential of such a dipole of momentum $\overrightarrow{\mu}(\mu_x,\mu_y)$, located at $\mathbf{M_{dip}}(x_{dip},z_{dip})$, writes in finite depth in the frequency domain (see Guével *et al* [5]): $\widetilde{\phi}_{dip} = \overrightarrow{\mu}.\overrightarrow{grad}_{\mathbf{M_{dip}}}\widetilde{F}(\mathbf{M},\mathbf{M_{dip}})$

with $\widetilde{F}(\mathbf{M},\mathbf{M_{dip}}) = -i\dfrac{M_0^2-K_0^2}{M_0(M_0^2-K_0^2+K_0)}ch[M_0(z+1)]ch[M_0(z_{dip}+1)]e^{iM_0|x-x_{dip}|} + \widetilde{F}_{evan}(\mathbf{M},\mathbf{M_{dip}}) \quad , \quad \mathbf{M}(x,z)\in D \qquad (5)$

and where $\widetilde{F}_{evan}$ is an evanescent function we neglect. Imposing in addition $\widetilde{\eta} = i\omega\widetilde{\phi}_{dip} = i\omega(\mu_x\partial\widetilde{F}/\partial x_{dip} + \mu_z\partial\widetilde{F}/\partial z_{dip}) = 0$ when $x < x_{dip}$ in (5), one deduces the following condition on the dipole momentum

$$\mu_x = ith[M_0(z_{dip}+1)]\mu_z \qquad (6)$$

We will call 'optimal submerged dipole' a Rankine dipole whose momentum $\overrightarrow{\mu}$ verifies this condition (6). Hence, outside the evanescent zone occurring right on top of this kind of linear dipole, it generates no wave in the negative x direction and a regular wave train at its frequency towards the positive x, whose amplitude is

$$A(\omega) = 2\mu_z\sqrt{K_0}\,\frac{M_0^2-K_0^2}{M_0^2-K_0^2+K_0}\cosh[M_0]\cosh[M_0(z_{dip}+1)] \qquad (7)$$

Figure 1 compares this theoretical amplitude to the ones simulated at different frequencies by the spectral model, utilized with a Rankine dipole of same momentum and with very small amplitudes (i.e. in linear conditions). An excellent agreement is found between numerical and analytical wave generation transfer functions. The analytical potential used in the model is eventually written as

$$\phi^{dipoles}(\mathbf{M},t) = R(t)A(\omega)\sum_{k=0}^{N_{images}}\frac{th[M_0(z_{dip_k}+1)]\cos(\omega t)(x-x_{dip_k}) + \sin(\omega t)(z-z_{dip_k})}{(x-x_{dip_k})^2+(z-z_{dip_k})^2} \quad , \quad \mathbf{M}\in D \qquad (8)$$

in which a sum on the dipole images appears, required to take into account the presence of side and bottom walls. And $R(t)$ is a smooth time ramp applied to the first period of the generation.

One of the first studies on the generation of unidirectional waves by means of submerged dipoles was due to Clément [6]. Having obtained satisfactory results with a circular spinning dipole in deep water (considering the dipole momentum vector in the vertical plane, it spins in time), he proposed a heuristic extension for finite depth cases. This consisted in forcing the dipole momentum to reproduce locally the physical (horizontal major axis) elliptic motion of the particles under a unidirectional wave train. This so-called 'spinning dipole' technique managed to reduce largely the waves generated towards negative x but not totally, and the result was depending on the depth of submersion and of the frequency. In contrast, with our 'optimal submerged dipole' derived from linear finite depth theory, we actually obtain no propagating wave field to the x negative in all the cases simulated (cf. the results section); and taking a closer look at the dipole momentum vector motion we find also an ellipse, but whose major axis is *vertical* this time.

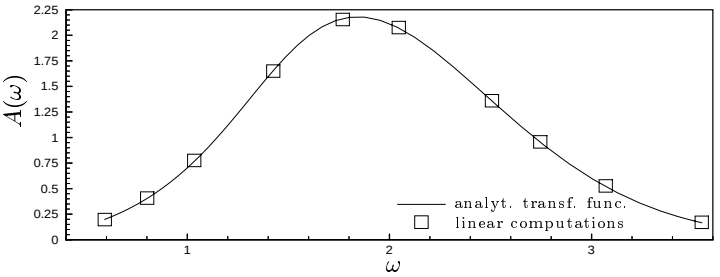

Fig.1 Linear amplitude of the wave generated by a single dipole.

Unsteady case. The first idea to generalize this monochromatic formulation is to superpose dipoles of different frequencies and phases, so as to generate unsteady wave patterns such as sea states. The spectrum of the sea state is then divided into bands of frequency with one dipole per band. This has been realized recently and coupled to a $3D$ diffraction code to simulate a sea state impinging on a vertical cylinder (see Ferrant & Le Touzé [7]).

Another possible extension is to reproduce a given water elevation signal recorded at a distance of the wave generator. To reach this aim we first realize the spectral analysis of the target signal by Fourier Transform. Then the precedent transfer function $A(\omega)$ of the optimal dipole is employed to determine its momentum $\widetilde{\mu}$ in the frequency domain, including the phase shift linked to the distance to the target Δx: $\widetilde{\mu}(i\omega) = \widetilde{\eta}_{probe}(i\omega)/(A(\omega)e^{-k\Delta x})$ with k the wavenumber associated to the pulsation ω through the linear dispersion equation. Finally, we re-construct the time evolution of the optimal dipole momentum by inverse Fourier Transform. The resulting aperiodic momenta $\mu_x(t)$, $\mu_z(t)$ then replace the periodic ones of the monochromatic case in (8). It should here be highlighted that although its momentum varies unsteadily in time this dipole is still optimally adapted in a linear sense. Figure 2 represents the trace of such a momentum vector, located where the dipole lies in the tank. Its complicated motion reflects the unsteadiness of the wave field generated (in the circumstances a focused wave train).

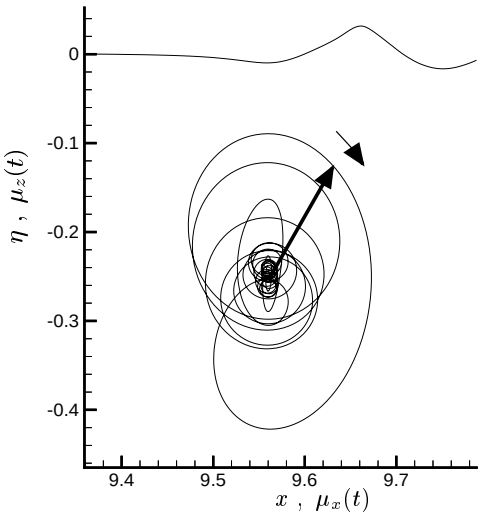

Fig.2 Example trajectory of the momentum vector of the unsteady optimal dipole (vector end is tracked).

NUMERICAL RESOLUTION

Spectral resolution. In the boundary-value problem previously described (equations (1) to (3)), the only unknowns are the so-called 'modal time amplitudes' $a_m(t)$ and the free surface elevation $\eta(x,t)$. The pseudospectral formulation (4) satisfies intrinsically Laplace's equation (1) and homogeneous Neumann conditions. Remaining free surface conditions (2) and (3) are then discretized at N_η collocation nodes. To update the unknowns, we use a 4^{th}-order Runge-Kutta time-marching scheme. The knowledge of the a_m-unknowns at $t+\Delta t$ requires the resolution of a $N_\eta \times (N_\phi+1)$ linear system assembled from the dynamic condition (3) taken at the N_η collocation nodes. In all the simulations shown a square system ($N_\eta = N_\phi + 1$) is solved by means of a GMRES method, except for the steepest case in regular waves where a 2-times overdetermination is chosen ($N_\eta = 2N_\phi + 1$) to help stability of the result; the linear system is there solved through an Householder method.

Wave generation. In monochromatic cases the dipole momentum is straightforwardly obtained. When we apply the unsteady scheme described above, more precautions shall be taken. Indeed a compromise is to be found in the choice of the frequency window

in the discrete Fourier Transform, on one hand we need to keep sufficiently high frequencies to reproduce properly the target signal, and on the other hand we want to avoid numerical problems raising where the dipole transfer function goes to zero (because of the division in $\widetilde{\mu}(i\omega)$). As for low frequencies, no such problems appear. A solution is to place the dipole closer to the free surface, which shifts its transfer function towards the highest frequencies, but in that case the evanescent field produced provokes other difficulties in nonlinear cases (see results section). Eventually, a depth $z_{dip} = -0.4$ and a pulsation window of $[0.25, 5.2]$ have been selected, $\omega = 5.2$ being sufficient to be very close to the target in linear. An alternative to get rid of this difficulty might be found in the splitting of the frequency window into 2 (or even more) bands, each being taken in charge by a different dipole submerged at a relevant depth. This will be tried soon and presented at the workshop.

ILLUSTRATIVE RESULTS

Generation of Regular Waves

In order to check the efficiency of our dipole optimization, we have first proceeded to the simulation of regular wave trains in the tank. The features under question on this simple case were first the unidirectionality of the waves as cases deviate from linear conditions, and more generally the stability of the generation method on strongly-nonlinear cases.

An example of the results obtained is shown on figure 3: a $\lambda = 0.5$ wave train is generated in a $L_x = 10$ long tank by means of one monochromatic optimal dipole located at $(x_d = 2.5, z_d = -0.25)$ (materialized by a thick dot on the last plot). The established wave patterns are presented for three different steepness, with the steepness ε being defined as the ratio of the wave height $H = \eta_{crest} - \eta_{trough}$ to the wavelength λ. The first plot is a quasi-linear case ($\varepsilon = 1\%$), the next two are respectively nonlinear ($\varepsilon = 5\%$) and 'strongly nonlinear' ($\varepsilon = 10\%$). Parabolic absorption applies in the first and last fifth of the tank. 193 modes and 30 time steps per period are selected, parameters far sufficient to ensure converged results. For an easier visual comparison, the three plots follow the same representative scale with respect to their steepness.

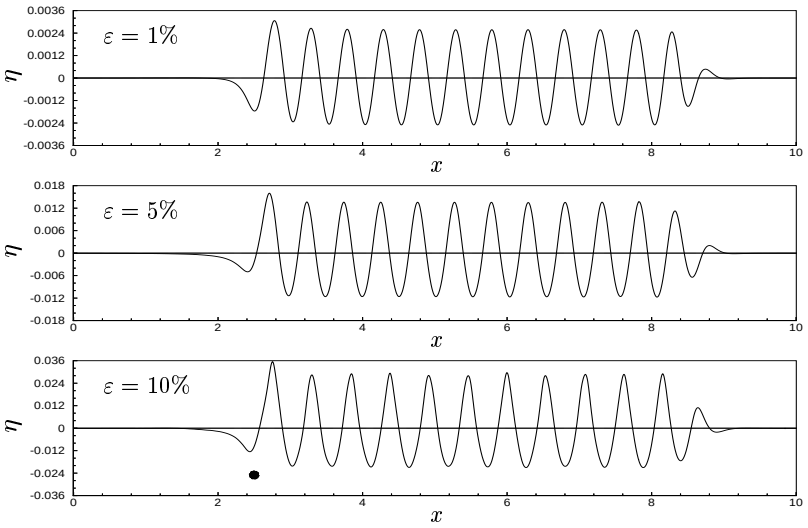

Fig.3 Steady regular wave patterns in the tank for 3 different steepness.

The first conclusion to be drawn is the noticeable absence of waves generated to the left, and this for all the three steepness. The optimization proves therefore its efficiency even for strongly nonlinear waves, at least in steady cases. The other appreciable result resides in the wave pattern itself which appears very regular and proved to be stable in time as well; typical nonlinear characteristics are observable as steepness increases, such as higher crests than troughs, steeper crests, etc.

Reproduction of Focused Wave Packets

Once verified the wave generation using an optimized steady dipole, the case of an unsteady target wave pattern has been investigated. As quoted in the formulation section, the aim here is to reproduce the time evolution of the water elevation recorded at a probe settled in the tank. A zoom of the target record chosen is shown on figure 4, elsewhere in the [0 , 36.4] time window the target water elevation is null. This focused wave packet impinging on a bottom-mounted cylinder is a case that has been studied experimentally in the framework of CLAROM project. The wave tank we simulate corresponds to the one tested in the experience, with a target at $30m$ from the wave generator for a water depth of $2.90m$. In the plots the target location is materialized by a vertical dotted line at $x = 20$; the unsteady submerged dipole is located at $(x = 9.56, z = -0.4)$ (the other dotted line). The corresponding trajectory of the temporal dipole momentum vector is shown on figure 2.

Parabolic absorption applies in the first and last fourth of the tank, The $[\omega = 0.25, \omega = 5.2]$ window selected to operate the Fourier Transform corresponds to wavelengths from a few centimeters to the tank length. Thanks to the 'spectral convergence' a relatively moderate number of modes, 193, is sufficient to ensure converged simulations. The same number of collocation nodes is employed; with a spline interpolation between calculation nodes applied for the figures. A converged time step of 0.1 is selected, so that the shortest wave generated counts about 12 time steps per period. As a result, those simulations are not only precise, but also reasonably fast (about 10 minutes on a 1GHz-Pentium processor for 1000 time steps).

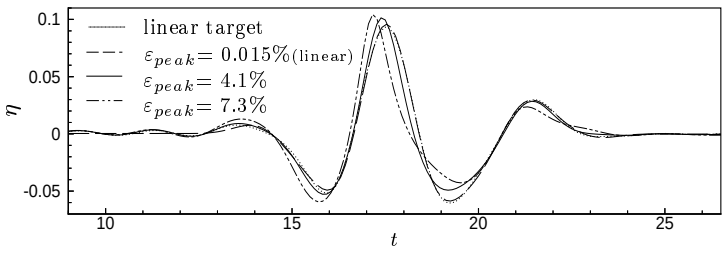

Fig.4 Target, linear and nonlinear peaks recorded at the probe (scaled by the '7.3%-case' amplitude factor).

Results for three different amplitudes are discussed hereafter: the first one is a linear case (very low amplitude corresponding to an $\varepsilon_{peak} = 0.015\%$ local steepness at the peak), and the two others are fairly nonlinear when the focusing occurs ($\varepsilon_{peak} = 4.1\%$ and 7.3%). The 'local steepness at the peak' defined as $(\eta_{peak\ crest} - \eta_{peak\ trough})/(2(x_{peak\ trough} - x_{peak\ crest}))$ is used to quantify the nonlinearity of the peak. Another significant criterion is the maximum slope on the peak sides.

The linear case is selected to make sure of the validity of our model on its whole. Indeed, if the result provided by the loop 'Fourier Transform of the signal/determination of the unsteady dipole momentum/linear temporal generation and focusing' matches back the target, the method is consistent. It is actually the case since target and recorded signals at the probe are almost superposed (and would be with a wider frequency window) on figure 4, that plots the water elevation evolution at this location for the different amplitudes simulated. Hence, the linear case is a valuable reference to study the influence of nonlinearites. The quantification of the

nonlinearities involved in the two nonlinear cases lead respectively to local steepness of 4.1% and 7.3%, and maximum slopes of 18% and 39%, confirming their importance. Those quantities are measurable on figure 5 which represents the peaks shapes in space at their maximum locations, normalized by the linear maximum (dotted horizontal line).

Figure 6 presents snapshots of the free surface at different times of the linear and nonlinear wave packets propagation, including the focusing and the start of the following dispersion. First, one can check once again that the unidirectionality of the waves remains very satisfactory in this case as well. Moreover, except a little perturbation appearing in the late stage of the nonlinear wave generation, the deformations are very similar in the two cases before focusing occurs. This phenomenon was expected since the focusing principle is relying on this very fact that moderate amplitude waves of different wavelengths can superpose temporarily to produce a much steeper wave. However a little perturbation appears in the nonlinear case, due to observed local steep water deformations right on top of the dipole where evanescent waves are not negligible. The relative perturbation on the '7.3%-case' is twice as big, which is still acceptable, but we stay dubious about our steeper run cases (up to 15%). The mentioned split of the frequency window should help. Even though, this high frequencies perturbation being much slower than the desired long waves along with it is generated, it does not reach the probe before the end of the time target window $t = 36.4$.

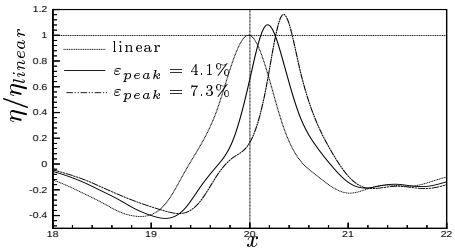

Fig.5 Linear and nonlinear peaks spatial shapes at their respective maxima (scaled by linear case).

If one now takes a closer look at figure 4, a little shift in time of the peak can be observed, gaining advance as nonlinearities increase. This might be correlated to the reduction in nonlinear regular wave periods as their steepness increases. We note also a typical raising of the crest and troughs, however the relative maximum of the strongest case appears is not relatively higher than in the '4.1%-case', surprisingly. This interrogation finds its answer in figure 5 where it is noticeable that the 'true' peak (defined as the time of maximum water elevation) has shifted in space and appears further from the probe. On this figure, one actually finds back the increase in relative maxima along with the local steepness.

Globally, the generated wave packet reproduces very satisfactorily the focused target signal in linear simulations, and its use in fully-nonlinear cases provides us with a focused wave presenting typical nonlinear characteristics. This solution will be coupled to our $3D$ fully-nonlinear diffraction model in the very near future, as it has been done before (Ferrant & Le Touzé [7]). This spectral model properties of rapid convergence and continuity of the solution across the free surface make it the relevant tool to realize such a $2D$-spectral incident/$3D$-diffracted model. Comparison to wave loads measured experimentally in the CLAROM project shall be realized as well. Another future development could consist in iterating on the difference between the nonlinear signal obtained at the probe and the target one, so as to converge towards the target for any amplitude of it.

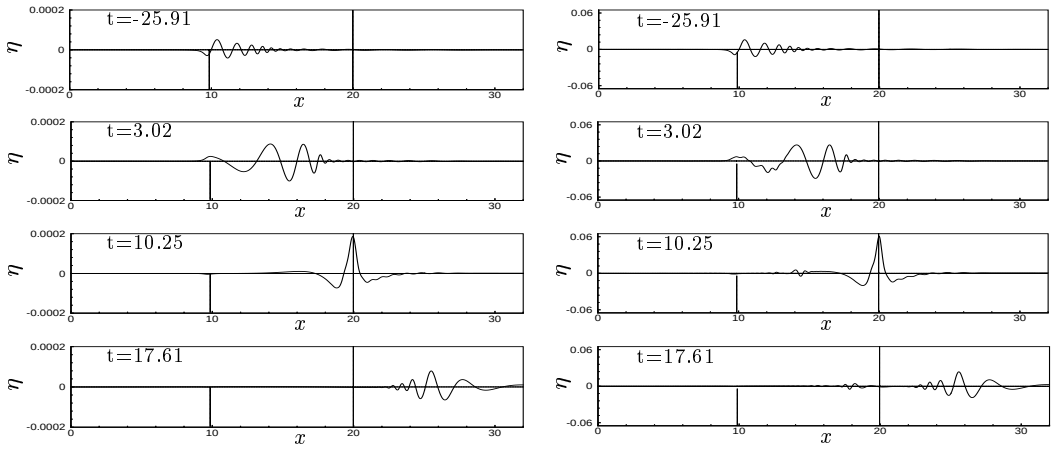

Fig.6 Snapshots of the free surface at 4 times of the generation -*left*: linear, *right*: $\varepsilon_{peak} = 4.1\%$.

CONCLUSION

In this paper, an optimization of submerged dipoles to generate a unidirectional wave train is derived and proves to work properly in linear cases as well as in strongly nonlinear ones. The presented spectral model including an optimized steady spinning dipole is shown to simulate stable regular steep wave patterns. An extension of the dipole generation process to the reproduction of unsteady target signals in the tank is proposed, and is applied to the case of a focusing wave train. This original method is validated on the linear case and results for sharp nonlinear peaks are produced and commented. The method exhibits the usual performances of spectral schemes, with respect to accuracy and rate of convergence. The solution appears to be reliable, precise and fast, and will soon be coupled to simulate the diffraction of such focused wave trains on a $3D$ body.

REFERENCES

[1] D.G. Dommermuth & D.K.P. Yue, 'A high-order spectral method for the study of nonlinear gravity waves', *J. Fluid Mech.* **184**, 267-288, (1987).

[2] R.W. Yeung & X. Yu, 'Three-dimensional Free-Surface Flow with Viscosity: A Spectral Solution', *Hydrodynamics in ship and ocean engineering*, RIAM, Kyushu University Publisher, Japan, 87-114, (2001).

[3] D. Le Touzé, F. Bonnefoy & P. Ferrant, 'Second order spectral simulation of directional wave generation and propagation in a 3D tank', *Proc. 12^{th} Int. Symp. on Offshore and Polar Engng*, Kitakyushu, Japan, (2002).

[4] J. Grue & M. Huseby, 'On the occurence of strong higher harmonic wave forces and induced ringing loads on vertical cylinders', *Proc. 21^{st} Int. Conf. on Offshore Mech. and Artic Engng*, Oslo, Norway, OMAE2002-28526, (2002).

[5] P. Guével *et al*, 'La récupération de l'énergie des vagues', *Sciences et Techniques de l'Armement - Mémorial de l'Artillerie Franaise*, Tome 60, n232, 17-207, (1986).

[6] A.H. Clément, 'The spinning dipole: an efficient unsymmetrical numerical wavemaker', *Proc. 14^{th} Int. Workshop on Water Waves and Floating Bodies*, Port Huron (MI), USA, 29-32, (1999).

[7] P. Ferrant & D. Le Touzé, 'Fully-nonlinear spectral/BEM solution for irregular wave interactions with a $3D$ body', *Proc. 21^{st} Int. Conf. on Offshore Mech. and Artic Engng*, Oslo, Norway, OMAE2002-28521, (2002).